THE JOURNAL OF
PHYSICAL CHEMISTRY
LETTERS
A JOURNAL OF THE AMERICAN CHEMICAL SOCIETY

pubs.acs.org/JPCL Letter

Simplified Tuning of Long-Range Corrected Time-Dependent Density Functional Theory

Aniket Mandal and John M. Herbert*

Cite This: *J. Phys. Chem. Lett.* 2025, 16, 2672−2680 Read Online

ACCESS | Metrics & More | Article Recommendations | Supporting Information

ABSTRACT: Range-separated hybrid functionals have dramatically improved the description of charge-transfer excitations in time-dependent density functional theory (TD-DFT), especially when the range-separation parameter is adjusted in order to satisfy the ionization energy (IE) criterion, $\varepsilon_{\mathrm{HOMO}} = -\mathrm{IE}$. However, this "optimal tuning" procedure is molecule-specific, inconvenient, expensive for large systems, and problematic in extended or periodic systems. Here, we consider an alternative procedure known as global density-dependent (GDD) tuning, which sets the range-separation parameter in an automated way based on properties of the exchange hole. In small molecules, we find that long-range corrected functionals with either IE or GDD tuning afford remarkably similar TD-DFT excitation energies, for both valence and charge-transfer excitations. However, GDD tuning is more efficient and is well-behaved even for large systems. It provides a black-box solution to the optimal-tuning problem that can replace IE tuning for many applications of TD-DFT.

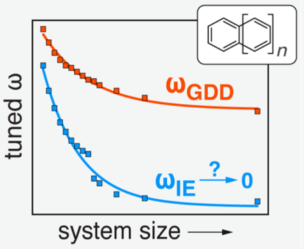

With its favorable balance of accuracy and affordability, time-dependent density functional theory (TD-DFT) has become the method of choice for excited-state calculations in molecules with more than 10−20 atoms.[1] Early applications of TD-DFT noted egregious failures for Rydberg and charge-transfer (CT) excitations,[2−8] ultimately traceable to incorrect asymptotic dependence of the exchange-correlation potential, v_{xc}.[9−11] That behavior can be rectified using long-range corrected (LRC) exchange functionals,[12−15]

$$E_{\mathrm{x}}^{\mathrm{LRC}} = (1 - c_{\mathrm{hfx}})E_{\mathrm{x,GGA}}^{\mathrm{SR}} + c_{\mathrm{hfx}}E_{\mathrm{x,HF}}^{\mathrm{SR}} + E_{\mathrm{x,HF}}^{\mathrm{LR}} \tag{1}$$

Here, $E_{\mathrm{x,GGA}}^{\mathrm{SR}}$ is a short-range exchange functional obtained from a generalized gradient approximation (GGA),[14−16] while the quantities $E_{\mathrm{x,HF}}^{\mathrm{SR}}$ and $E_{\mathrm{x,HF}}^{\mathrm{LR}}$ are short- and long-range Hartree−Fock exchange, respectively.

This range separation is based on partition of the Coulomb operator, the most widely used form of which is[1]

$$\frac{1}{r_{12}} = \underbrace{\frac{1 - \mathrm{erf}(\omega r_{12})}{r_{12}}}_{\mathrm{SR}} + \underbrace{\frac{\mathrm{erf}(\omega r_{12})}{r_{12}}}_{\mathrm{LR}} \tag{2}$$

This introduces one adjustable parameter (ω) whose value sets the length scale ($\sim 1/\omega$) for the asymptotic transition to exact exchange. It has been suggested to set ω in a nonempirical way,[17−22] based on the ionization energy (IE) theorem of exact DFT.[11,23,24] That condition,

$$\varepsilon_{\mathrm{HOMO}} = \underbrace{E(N) - E(N-1)}_{-\mathrm{IE}} \tag{3}$$

relates the highest occupied molecular orbital (HOMO) energy level to the IE. By tuning ω in order to satisfy eq 3, accurate CT excitation energies can be obtained.[17−20] This paradigm has been so successful that some have described the description of CT states in TD-DFT as a solved problem.[25]

The IE-tuning procedure described above, which is sometimes called "optimal" tuning,[20] is appealing because it is motivated by an exact condition. It starts from a model with correct asymptotic shape, since $v_{\mathrm{xc}}(r) \sim -1/r$ for any LRC functional with 100% long-range Hartree−Fock exchange, as in eq 1. Then, the correct asymptotic value $v_{\mathrm{xc}}(\infty)$ is enforced via eq 3.[11,26] We rewrite the latter condition as

$$\mathrm{IE}(\omega_{\mathrm{IE}}) = -\varepsilon_{\mathrm{HOMO}}(\omega_{\mathrm{IE}}) \tag{4}$$

which indicates what the procedure entails, namely, a sequence of LRC-DFT calculations for both the molecule and its cation, using different values of ω, in order to determine the optimal value ω_{IE} that satisfies eq 4. This is expensive for large molecules and tedious in any case, and there is no guarantee that such a value exists. In particular, IE-tuning can be fraught for small-gap systems, which drive the optimally tuned value of ω toward zero, corresponding to a functional that eliminates $E_{\mathrm{x,HF}}^{\mathrm{LR}}$. This small-gap behavior is noteworthy because semilocal GGA functionals tend toward vanishing gaps for large systems.[27−34] Problems with IE tuning have been observed in large conjugated π systems,[35−39] long-chain alkanes,[35] nanoscale materials,[40] and large water cluster anions.[41] For periodic systems, where introducing a net charge is problem-

Received: January 11, 2025
Revised: February 23, 2025
Accepted: February 28, 2025

https://doi.org/10.1021/acs.jpclett.5c00086

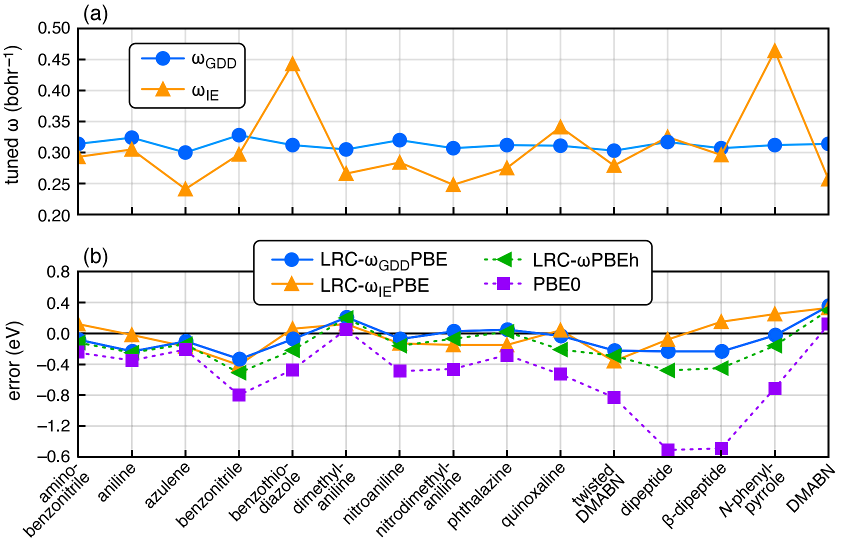

Figure 1. Results for a data set of transitions with charge-separated character. (a) Comparison of tuned range separation parameters (ω_{IE} and ω_{GDD}), obtained within the framework of the LRC-ωPBE functional. (b) Errors in TD-DFT excitation energies, with negative values indicating that the TD-DFT transition energy lies below the benchmark. All calculations use the def2-TZVPD basis set. Numerical data for 24 distinct transitions can be found in Table S1, including more than one transition for some of these molecules.

atic, IE tuning must be done carefully, based on localized orbitals.[42] The same procedure can also mitigate problems with IE tuning in long-chain polymers.[43]

In the present work, we consider TD-DFT applications using LRC functionals with an alternative (and automatic) means to determine ω, in a system-specific way, based on a global density-dependent (GDD) tuning procedure.[35] Here, the range-separation parameter is determined according to

$$\omega_{\text{GDD}} = C_{\text{GDD}} \langle d_{\text{x}}^2 \rangle^{-1/2} \tag{5}$$

where d_{x}^2 is the second moment of the distance to the center of the exchange hole, weighted toward asymptotic distances. (Details are provided in the Methods section.) The parameter C_{GDD} is empirical and is determined so that $\omega_{\text{GDD}} \approx \omega_{\text{IE}}$ for a data set of small molecules.[35,44,45] Nevertheless, we find that GDD tuning performs well on large molecules also, and is often negligibly different from IE tuning in TD-DFT applications. Meanwhile, it reduces the cost and increases the convenience to determine an optimal range-separation parameter.

We first compare the IE- and GDD-tuning approaches for TD-DFT calculations on CT excitation energies because that is the problem that LRC-DFT was originally designed to solve.[13] Tuned values ω_{IE} and ω_{GDD}, using the LRC-ωPBE functional,[46] are depicted in Figure 1a for a set of transitions with charge-separated character. (The complete data set can be found in Table S1, assembled from existing benchmarks.[47,48]) Optimal values ω_{GDD} are relatively constant across this data set whereas ω_{IE} exhibits larger molecule-by-molecule differences, especially for benzothiadiazole and *N*-phenylpyrrole. With the exception of those two cases plus quinoxaline and a dipeptide, $\omega_{\text{IE}} < \omega_{\text{GDD}}$.

Strikingly, these variations are not reflected in the TD-DFT excitation energies (Figure 1b). Even those molecules with the largest difference between ω_{IE} and ω_{GDD} exhibit very small differences in excitation energies (ca. 0.1 eV), indicating that excitation energies are not exquisitely sensitive to ω, at least not in the vicinity of the optimally tuned value. To set a baseline establishing that LRC functionals do improve the description of CT states, we also show TD-PBE0 errors in Figure 1b. These are much larger and tend toward significant underestimation of CT transition energies.

The LRC-ωPBE functional does not incorporate any exact exchange at short-range, meaning that $c_{\text{hfx}} = 0$ in eq 1. For comparison, we also examine the LRC-ωPBEh functional that uses $c_{\text{hfx}} = 0.2$ and sets $\omega = 0.2$ bohr^{-1} by fiat, based on empirical fitting.[49] TD-DFT results using this functional are similar to those obtained using the optimally tuned LRC-ωPBE functionals (Figure 1b). This is not surprising, given where the tuning procedures landed and the observed insensitivity to ω. Furthermore, these results indicate why LRC-ωPBEh is an effective choice for systems whose excited states exhibit charge-separated character.[49−51] It is interesting that LRC-ω_{GDD}PBE results hew more closely to LRC-ωPBEh than do the IE-tuned results.

Overall, error statistics are negligibly different for these three TD-LRC-DFT methods, as documented in Table 1. Errors are also negligibly different when LRC-ωPBEh is tuned with either the GDD or the IE procedure. The range-separated CAM-B3LYP functional[52] also performs well for this data set. It engenders more significant errors for larger molecules,[53] however, because CAM-B3LYP incorporates only 65% Hartree−Fock exchange at long-range.[52] (Problems with incorporating IE tuning into the CAM-B3LYP *ansatz* have been noted,[54] and we have not attempted it here.) TD-PBE0 and TD-B3LYP errors for CT excitations are limited only by the size of the molecule and are more dramatic in large molecules, solvated systems, and aggregates.[5−8,32,47,50]

Whereas the data set examined in Figure 1 consists of CT transitions, Figure 2 plots TD-DFT errors for a standard set of valence transitions.[47] (See Table S2 for the complete data set.) As a baseline comparison for GGAs and global hybrid functionals, we include TD-PBE and TD-PBE0 results alongside TD-LRC-ωPBE using ω_{IE} or ω_{GDD} for the range-separation parameter. Significant and systematic underestimation of excitation energies using GGA functionals (including but not limited to PBE) is a common side effect of incorrect asymptotic behavior of $v_{\text{xc}}(r)$.[1] Global hybrid functionals such

https://doi.org/10.1021/acs.jpclett.5c00086
J. Phys. Chem. Lett. 2025, 16, 2672−2680

Table 1. TD-DFT/def2-TZVPD Error Statistics for CT Transitions[a]

Method	Error (eV)[b]		
	MAE[c]	Mean	Max
LRC-ωPBE[d,e]	0.19	−0.01	0.45
LRC-ω_{IE}PBE[d]	0.19	0.07	0.71
LRC-ω_{GDD}PBE[d]	0.18	0.01	0.46
LRC-ωPBEh[f,g]	0.22	−0.07	−0.48
LRC-ω_{IE}PBEh[f]	0.20	−0.04	0.46
LRC-ω_{GDD}PBEh[f]	0.20	0.17	0.57
CAM-B3LYP	0.20	−0.12	−0.75
PBE0	0.52	−0.48	−1.49
B3LYP	0.65	−0.64	−1.87

[a] For the data set of 24 transitions in Table S1. [b] With respect to benchmarks in Table S1, taken from refs 47 and 48. [c] Mean absolute error. [d] $c_{\text{hfx}} = 0$. [e] $\omega = 0.3$ bohr^{-1} (no tuning). [f] $c_{\text{hfx}} = 0.2$. [g] $\omega = 0.2$ bohr^{-1} (no tuning).

as PBE0 push the excitations energies higher, resulting in typical unsigned errors of 0.2−0.3 eV for localized excitations,[1,55] which is smaller than typical errors for CT transitions. These trends are reflected in the TD-PBE and TD-PBE0 data in Figure 2.

As compared to global hybrids, LRC functionals stabilize the occupied energy levels. Functionals whose range separation parameters are fit to thermochemical data tend to push even localized excitation energies somewhat higher, which slightly upsets the good performance of methods such as TD-PBE0 for valence excitation energies, leading to typical errors of 0.3−0.4 eV when LRC functionals are employed.[1,55] CAM-B3LYP avoids this degradation by sacrificing the LRC constraint of 100% exact exchange at long range,[51,52] meaning that $v_{\text{xc}}(r)$ decays somewhat too quickly for a charge-separated excitation. For the tuned LRC-ωPBE functionals, which maintain correct asymptotic behavior, any upshift in the valence excitation energies is a small effect, as the average errors are comparable to those exhibited by PBE0 (Figure 2).

The tuned functionals LRC-ω_{IE}PBEh and LRC-ω_{GDD}PBEh with $c_{\text{hfx}} = 0.2$ afford very similar error distributions as compared to the corresponding functionals with $c_{\text{hfx}} = 0$, as shown in Figure 2. For non-LRC functionals, however, increasing the amount of exact exchange has a significant impact on the mean signed error (MSE) for these localized excitations. TD-PBE calculations systematically underestimate excitation energies, which is typical of semilocal functionals,[1,55] with a MSE of −0.45 eV for this data set. For TD-PBE0, the MSE is reduced to −0.13 eV and the mean absolute error (MAE) is 0.24 eV, which is as good as any standard functional for typical small-molecule benchmarks.[1] MAEs for the tuned LRC functionals are similar but the MSEs are positive, consistent with a small upward shift in the excitation energies as compared to TD-PBE0. Finally, the HF-PBE functional,

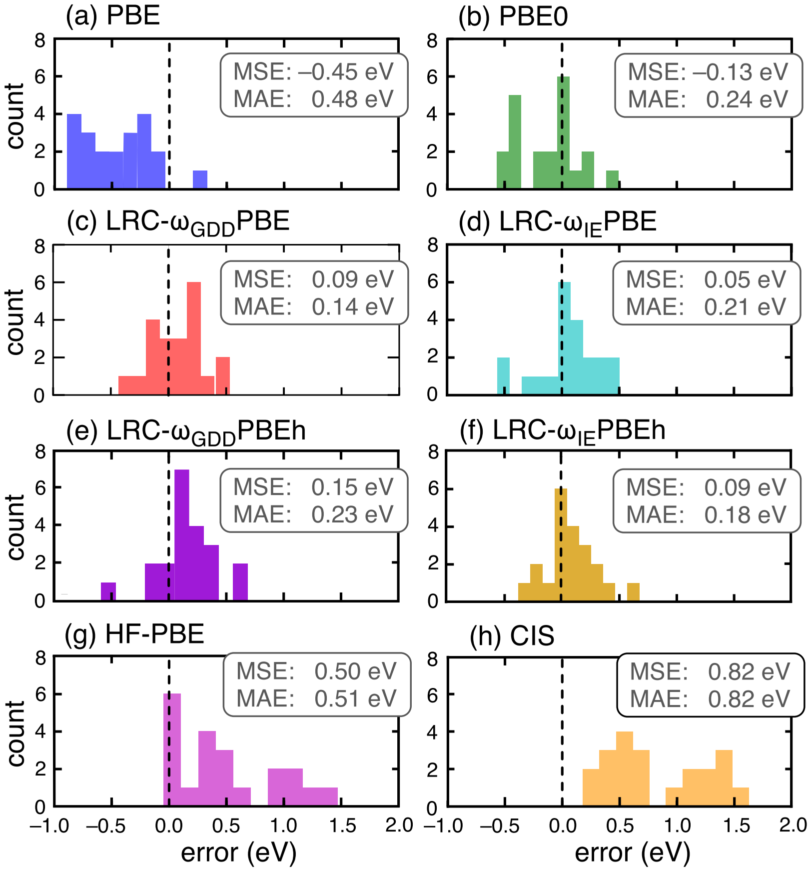

Figure 2. Errors in TD-DFT/def2-TZVPD excitation energies (with respect to established benchmarks), for a data set of valence excitations from ref 47, using the functionals (a) PBE, (b) PBE0, (c) LRC-ω_{GDD}PBE, (d) LRC-ω_{IE}PBE, (e) LRC-ω_{GDD}PBEh, (h) LRC-ω_{IE}PBEh, (g) HF-PBE, and (h) CIS. Numerical data can be found in Table S2.

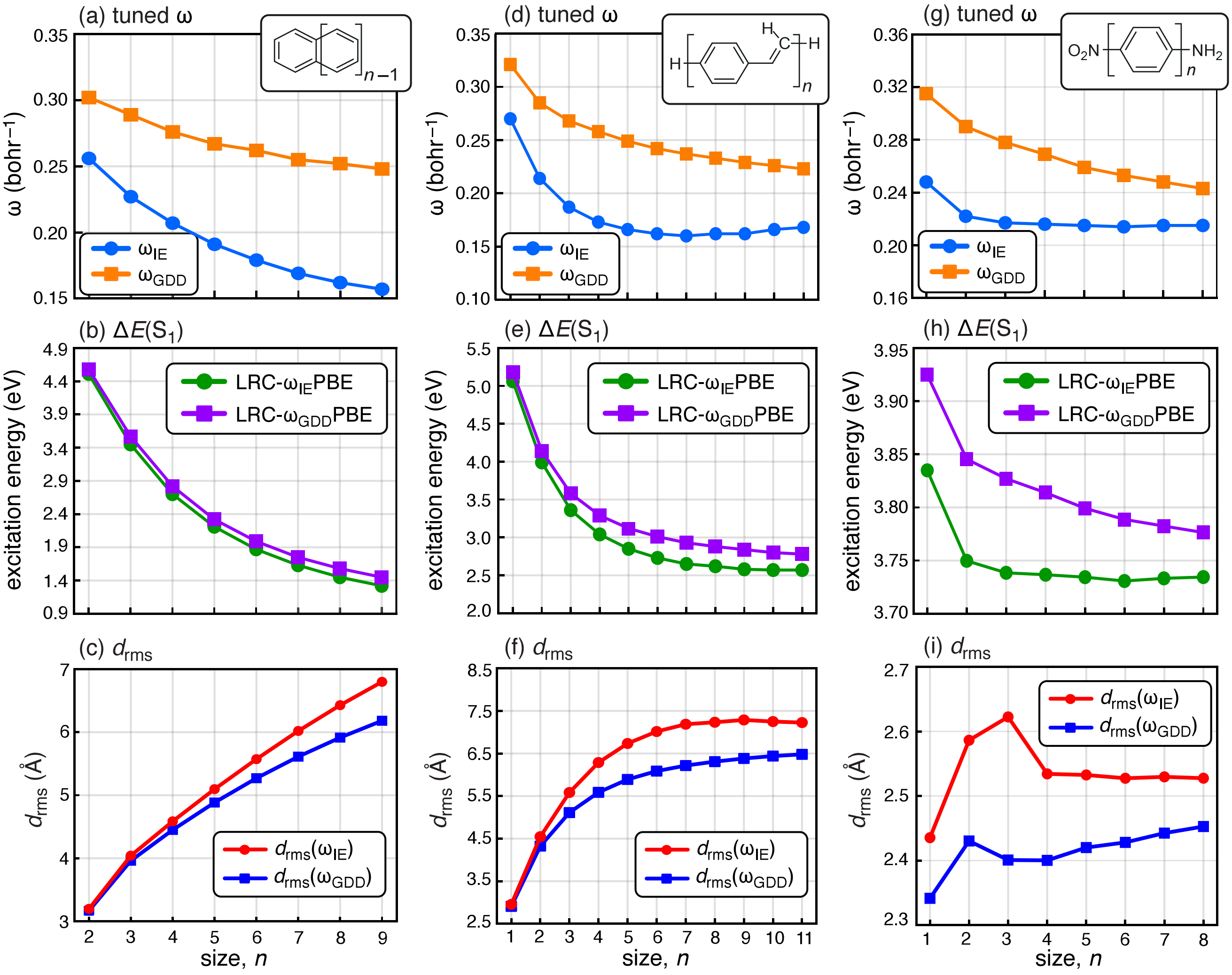

Figure 3. Tuned LRC-ωPBE results for conjugated polymers as a function of molecular size. (a) Optimal ω values, (b) TD-DFT(TDA) excitation energies for the S_1 state, and (c) exciton size for linear acene molecules. (d) Optimal ω, (e) $\Delta E(S_1)$, and (f) d_{rms} for $(PPV)_n$ oligomers. (g) Optimal ω, (h) $\Delta E(S_1)$, and (i) d_{rms} for $O_2N(Ph)_nNH_2$. Acene calculations were performed using the def2-TZVPD basis set and other calculations used def2-ma-SVP.

$$E_{xc}^{\text{HF-PBE}} = E_x^{\text{HF}} + E_c^{\text{PBE}} \qquad (6)$$

sets an opposite goalpost as compared to TD-PBE. It exhibits a MAE of 0.51 eV and nearly all of the errors are positive. For comparison, the uncorrelated configuration interaction singles (CIS) method affords strictly positive errors with a MAE of 0.82 eV.

Description of the ^1L_a transition of the linear acene molecules is a trouble spot for TD-DFT, even with global hybrid functionals.[56] Errors increase as a function of molecular size in a manner that is not observed for the ^1L_b state, which is polarized along the opposite axis of the molecule.[50,56] As compared to either GGA or hybrid functionals, LRC functionals do a much better job at describing both states.[50] Optimal tuning affords especially accurate excitation energies, with MAEs of 0.17 eV (LRC-ω_{IE}PBE) and 0.20 eV (LRC-ω_{GDD}PBE) with respect to experiment, considering the combined data set of ^1L_a and ^1L_b for naphthalene through hexacene (Table S3). For naphthalene, the ^1L_b state lies below ^1L_a, in contrast to the behavior for the larger acenes, and this is captured by both of the aforementioned LRC functionals but not by PBE, PBE0, or HF-PBE. Most importantly for the present analysis, TD-DFT excitation energies obtained using LRC-ω_{IE}PBE versus LRC-ω_{GDD}PBE differ by an average of only 0.12 eV, which is smaller than the intrinsic accuracy of either method.

Although these two tuned LRC functionals perform equally well for acene excitation energies, they yield different results for other properties. HOMO/LUMO gaps for the acene sequence are known to decrease much faster than the corresponding gaps for the cyclohexane-based perhydroacenes,[57] and application of IE tuning to the linear acenes suggests that $\omega_{IE} \to 0$ as the number of rings increases.[39] (This is consistent with vanishing-gap behavior when GGA functionals are applied to other large insulators.[27−34]) The decay rate of ω_{IE} is much faster than that of ω_{GDD}, as shown in Figure 3a. The GDD-tuned value appears to be approaching a characteristic length scale $1/\omega_{GDD} \approx 4$ bohr that is comparable to the size of one benzene ring (4.645 bohr), whereas $1/\omega_{IE} > 4$ bohr except in the case of naphthalene. Problems with IE tuning in other one-dimensional polymers have been noted recently, with tuning based on localized orbitals as a suggested workaround.[43]

Size-dependent trends in the ${}^1L_a$ excitation energies are plotted in Figure 3b. Consistent with TD-LRC-ωPBE error statistics discussed above, the two tuning schemes afford very similar results although a slight difference emerges as the number of rings increases, with systematically lower excitation energies for IE tuning. However, the difference amounts to only 0.1 eV for nonacene, which is smaller than the inherent accuracy for acenes where benchmarks are available, despite a significant difference between ω_{IE} and ω_{GDD}. This situation is reminiscent of the CT data in Figure 1, where modest differences between ω_{IE} and ω_{GDD} did not manifest as significant differences in excitation energies.

Upon extending these calculations to larger acenes, we observe a discontinuity in the HOMO/LUMO gap computed using LRC-ωPBE, between $n = 10$ and $n = 11$ rings. The S_1 excitation energy and ω_{IE} exhibit corresponding discontinuities as shown in Figure S2. The discontinuity in ω_{IE} is attributable to the abrupt change in the Kohn–Sham gap, yet there is no discontinuity in ω_{GDD} (Figure S2a). Nevertheless, there is a discontinuity in the S_1 excitation energy computed using TD-LRC-ω_{GDD}PBE, which is similar to that obtained using TD-LRC-ω_{IE}PBE (Figure S2b). This behavior, along with extremely small (sometimes negative) excitation energies starting at $n = 11$, points to instabilities in the ground-state calculation. These TD-DFT calculations were performed using the Tamm-Dancoff approximation (TDA),[1] as full linear response exhibits imaginary eigenvalue problems for the larger acenes. All of this hints at the appearance of an open-shell biradicaloid singlet ground state for larger acenes. This has been discussed in the literature[58,59] but lies beyond the scope of ω-tuning.

For other conjugated polymers, the two tuning procedures engender larger differences in excitation energies. Figure 3 also presents data for a sequence of poly(p-phenylenevinylene)$_n$ or (PPV)$_n$ oligomers, as well as poly(p-phenyl)nitroaniline [$O_2N-(C_6H_4)_n-NH_2$], which we abbreviate as $O_2N(Ph)_nNH_2$. For (PPV)$_n$, the behavior is similar to that of the acenes in the sense that $\omega_{\text{IE}} < \omega_{\text{GDD}}$ for a given oligomer size, although in this case ω_{IE} seems to have converged by $n = 7$. There is a very slight upshift in ω_{IE} for larger oligomers, which is mirrored in the HOMO/LUMO gaps; see Figure S3e for the latter. At first, we hypothesized that this might arise due to a slight twisting of the PPV chain in the optimized geometries that we employ, yet the same behavior is evident in coplanar geometries of (PPV)$_n$. Furthermore, the uptick in ω_{IE} has no effect on the S_1 transition energies, which are plotted in Figure 3e. We conclude that small fluctuations around the asymptotic value of ω_{IE} reflect a degree of insensitivity to ω, in the vicinity of the optimally tuned value. Thus, the large-n behavior of ω_{IE} reflects the limitations in computing the optimal value of ω when the objective function is rather flat.

For the (PPV)$_n$ excitation energies, TD-LRC-ω_{IE}PBE and TD-LRC-ω_{GDD}PBE results gradually diverge from one another as a function of n, reaching a difference of 0.4 eV for $n = 7$, by which point both calculations have reached an asymptotic value of the S_1 excitation energy. Similar behavior is observed for the push–pull systems [$O_2N(Ph)_nNH_2$], although in that case the large-n values of the S_1 excitation energy differ by only 0.1 eV. Similar to (PPV)$_n$, however, we observe that ω_{IE} reaches an asymptotic value rather quickly (by $n = 3$), whereas ω_{GDD} continues to decrease even at $n = 8$ (Figure 3g). The S_1 excitation energies show a similar trend, with ω_{IE} reaching an asymptotic value by $n = 3$ whereas ω_{GDD} continues a downward trend through $n = 8$ (Figure 3h).

In an effort to understand these size-dependent trends, we computed the exciton size as measured by the root-mean-square (rms) electron–hole separation,[60,61]

$$d_{\text{rms}} = \langle \|\mathbf{r}_{\text{elec}} - \mathbf{r}_{\text{hole}}\|^2 \rangle^{1/2} \tag{7}$$

Results are plotted along the bottom of Figure 3 for the acenes, (PPV)$_n$, and $O_2N(Ph)_nNH_2$ systems. For the acenes, exciton delocalization (as measured by d_{rms}) continues to increase through the largest size examined, with no indication of a plateau (Figure 3c). This indicates complete delocalization and we believe this behavior is consistent with ω_{GDD} values that continue to decrease at least through $n = 20$ (see Figure S2a), despite the aforementioned ground-state instability.

The behavior of d_{rms} is quite different for the (PPV)$_n$ systems, as shown in Figure 3f. Regardless of which tuning procedure is used, the exciton size reaches an asymptotic value by $n = 9$ or 10, although that value differs by about 1.1 Å depending on whether ω_{IE} or ω_{GDD} is used. This is consistent with an asymptotic excitation energy that is reached for the same oligomer size (Figure 3e), and indicates a maximum value for the effective conjugation length.[36,62] Notably, GGA functionals afford complete exciton delocalization for (PPV)$_n$, rather than a finite exciton size.[62] This is inconsistent with correlated wave function calculations, whereas TD-DFT calculations based on LRC functionals afford the correct result.[62] This should provide a cautionary note for recent attempts to adjust ω based on exciton size,[63] which in any case should only be attempted using orbital-invariant measures of that size.[61]

To this, we can add that larger exciton sizes obtained using IE tuning, meaning that $d_{\text{rms}}(\omega_{\text{IE}}) > d_{\text{rms}}(\omega_{\text{GDD}})$ for a given oligomer size, are consistent with the fact that $\omega_{\text{GDD}} > \omega_{\text{IE}}$ (Figure 3d). The latter fact implies that the onset of exact exchange occurs on a shorter length scale for GDD tuning as compared to IE tuning, restricting the delocalization of the former relative to the latter. However, this distinction comes with only a modest difference in the S_1 excitation energies.

Turning to the $O_2N(Ph)_nNH_2$ oligomers, we note that there is significant twisting of the (Ph)$_n$ chain in the optimized geometries that we employ, leading to a fluctuation in d_{rms} as a function of size, which settles to an asymptotic value by $n = 4$ for ω_{IE} (Figure 3i). For GDD tuning, the d_{rms} values shows an upward trend after $n = 4$, suggesting a link between ω and electron–hole separation. For IE tuning, the asymptotic value of d_{rms} is about 0.1 Å larger than it is in the $n = 1$ case and for $d_{\text{rms}}(\omega_{\text{GDD}})$ the value stays between 2.4 and 2.5 Å after $n = 1$. These differences are much smaller than the 2.5 Å length scale of one phenyl ring, and we regard them as insignificant.

Next, we consider the performance of both tuning schemes for a benchmark set of small open-shell and "exotic" molecules.[64] Tuned TD-LRC-ωPBE results are listed in Table 2 and we observe large differences between ω_{IE} and ω_{GDD} in some cases, yet excitation energies are often quite similar. For example, in NH_2 the excitation energies differ by less than 0.1 eV even though the tuned ω values differ by 0.13 bohr^{-1}. For the NCO and OH radicals, however, TD-LRC-ω_{IE}PBE and TD-LRC-ω_{GDD}PBE excitation energies differ by 0.5 and 0.4 eV, respectively, and the ω_{IE} values are unusually large. Even more striking is the failure to determine ω_{IE} for the CN radical, for which IE tuning sends $\omega \to \infty$. In contrast,

Table 2. TD-DFT(TDA) Results for Open-Shell and Exotic Molecules[a]

	ω (bohr^{-1})		Error (eV)[b]	
Transition	GDD	IE	GDD	IE
BeF ($^2\Pi$)	0.388	0.496	0.04	0.04
BH_2 ($^2B_1$)	0.404	0.482	0.08	0.08
CN ($^2\Pi$)[c]	0.486	-	0.27	-
HCF ($^1A''$)	0.462	0.468	−0.09	−0.12
NH_2 ($^2A_1$)	0.531	0.659	−0.09	−0.09
NO ($^2\Sigma^+$)	0.505	0.600	−0.49	−0.39
OH ($^2\Sigma^+$)	0.437	1.547	0.14	0.67
NCO ($^2\Sigma^+$)	0.444	1.515	0.48	0.85
MAE			0.21	0.28

[a] LRC-ωPBE/def2-TZVPD. [b] With respect to theoretical best estimates from ref 64. Positive errors indicate that the TD-DFT transition energy is larger than the benchmark. [c] IE tuning is omitted because $\omega_{\mathrm{IE}} \to \infty$.

GDD tuning is well behaved and affords an accurate excitation energy for this species.

Unusually large (and in one case, divergent) values of ω_{IE} may reflect an attempt by the tuning procedure to mitigate self-interaction error in the ground state, effectively hacking the LRC-ωPBE *ansatz* to turn it into a short-range hybrid functional by making $1/\omega$ small. (Indeed, both ω_{IE} and ω_{GDD} are larger for this whole data set, as compared to values that are typical in closed-shell systems.) However, the LRC-ω_{IE}PBEh functional with $c_{\mathrm{hfx}} = 0.2$ exhibits similar pathologies for OH, NCO, and CN; see Table S8. Apparently, 20% exact exchange at short range is insufficient to avoid these unusually large values of ω_{IE}.

Finally, we examine the absorption spectrum of the hydrated electron, which has frequently been used to interrogate structural models of this unusual species,[65] often using TD-DFT calculations.[41,66−68] For this purpose we selected seven well-spaced snapshots from a QM/MM simulation,[41] with DFT regions extending to a radius of 7.5 Å and consisting of $(H_2O)_N^-$ with $N = 68$−76. Tuning was performed separately for each snapshot and the results are quite consistent across structures, with $\omega_{\mathrm{GDD}} = 0.246$−0.253 bohr^{-1} and $\omega_{\mathrm{IE}} = 0.146$−0.161 bohr^{-1}.

TD-DFT(TDA) absorption spectra are shown in Figure 4, each computed using a total of 15 excited states per snapshot, which is not enough to converge the "blue tail" at higher energies.[66] However, $\lambda_{\max}$ is adequately approximated using just three excited states, representing s → p transitions of a particle in a cavity.[65,66] The fact that $\omega_{\mathrm{GDD}} > \omega_{\mathrm{IE}}$ translates into a blue shift in the GDD-tuned spectrum, which is peaked at 2.3 eV as compared to 1.8 eV for the IE-tuned spectrum and 1.7 eV for the experimental spectrum.[69] (Average excitation energies reported here encompass the lowest three excited states, weighted by oscillator strength.) Similar results are obtained for two other functionals that have been applied to this problem in the past; see Figure S5. Interestingly, LRC-ω_{GDD}PBE violates the IE theorem in eq 3 by an average of 0.3 eV yet predicts vertical IEs that are within 0.1 eV of LRC-ω_{IE}PBE values, which satisfy the IE theorem by construction. This is further evidence of modest sensitivity to ω in the vicinity of the optimally tuned value.

In summary, two alternative tuning procedures have been examined for determining an optimal range-separation parameter in functionals such as LRC-ωPBE. Both procedures afford accurate excitation energies for transitions that exhibit charge-separated character, a major motivation for the development of LRC functionals and IE tuning.[13,17−19] For small molecules, $\omega_{\mathrm{IE}} \approx \omega_{\mathrm{GDD}}$, essentially by construction since a single adjustable parameter in the GDD procedure is fit to ω_{IE} data.[35,44,45] For large systems, the GDD procedure has a clear advantage in that it is a black-box, one-shot calculation that avoids a laborious scan over ω in order to determine ω_{IE}. For example, in molecules such as $O_2N(Ph)_8NH_2$ and $(PPV)_{11}$, the IE-tuning procedure is about six times more expensive as compared to GDD tuning in our present implementation. Moreover, ω_{GDD} remains well-behaved in systems where the HOMO/LUMO gap becomes small or behaves erratically. For neutral molecules, GDD tuning avoids the need to perform calculations on an ionized species, which can be an advantage for DFT under periodic boundary conditions.

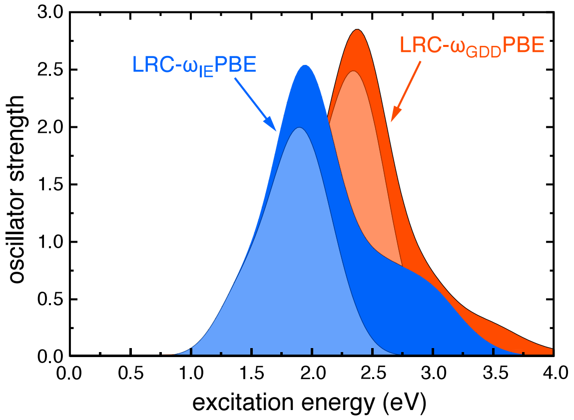

Figure 4. Simulated absorption spectra of e^-(aq) using seven QM/MM snapshots with 68−76 DFT water molecules and ≈18,000 classical point charges, as in ref 41. Vertical transition energies computed at the TD-DFT(TDA)/6-31++G* level were weighted by oscillator strength and broadened using a 0.2 eV Gaussian function. Darker spectra include 15 excited states while the lighter-colored spectra use only the lowest three excitation energies for each snapshot.

In many small-molecule cases, we find that TD-DFT excitation energies are surprisingly insensitive to ω in the vicinity of the optimally tuned value, so results using ω_{IE} versus ω_{GDD} are often statistically indistinguishable. For larger systems and some open-shell species, differences are more significant and the GDD procedure provides stable results even when the HOMO/LUMO gap is not well behaved, which is problematic for IE tuning. Overall, we find GDD tuning to be a simple replacement for IE tuning that offers advantages in many situations. It is already used routinely in some ground-state applications of LRC-DFT,[39,70] and we encourage its widespread use in TD-DFT calculations as well.

■ METHODS

All calculations were performed using Q-Chem,[71] in which GDD tuning was previously implemented.[44] This approach is based on the notion that the average distance between the exchange hole and the outermost electron in a molecule ought to determine the length scale (∼$1/\omega$) on which LRC is activated.[35] Operationally, this is implemented by computing the second moment of the exchange hole,[35,39]

$$\langle d_x^2 \rangle = \frac{\int \rho(\mathbf{r}) w(\mathbf{r}) d_x^2(\mathbf{r}) d\mathbf{r}}{\int \rho(\mathbf{r}) w(\mathbf{r}) d\mathbf{r}} \tag{8}$$

weighted towards asymptotic regions of the molecule using a function $w(\mathbf{r})$. The latter is taken to be[35]

$$w(\mathbf{r}) = \begin{cases} 1, & t(\mathbf{r}) \le \mu \\ 0, & t(\mathbf{r}) > \mu \end{cases} \tag{9}$$

where $t(\mathbf{r})$ is Becke's orbital localization function.[72,73] In the context of eq 9, $t(\mathbf{r})$ ensures that $w(\mathbf{r}) \approx 0$ in the region of localized orbitals. The parameter μ is determined self-consistently so that[35]

$$\int \rho(\mathbf{r}) w(\mathbf{r}) d\mathbf{r} = 1 \tag{10}$$

Finally, the parameter $C_{\text{GDD}} = 0.885$ in eq 5 was determined for use with LRC-ωPBE, in order to reproduce IE-tuning results.[44] That value is used throughout this work. Smaller values of C_{GDD} have been optimized for LRC functionals with $c_{\text{hfx}} > 0$.[35,45]

Since both $w(\mathbf{r})$ and $d_x^2(\mathbf{r})$ are functionals of $\rho(\mathbf{r})$, GDD tuning must be seeded with a self-consistent DFT calculation.[35] As in previous work,[39] LRC-ωPBE with $\omega = 0.3$ bohr^{-1} is used for that purpose. The density thus obtained is used to evaluate $\langle d_x^2 \rangle$ in eq 8, and the value of μ in eq 9 is determined iteratively in order to satisfy eq 10. At the conclusion of this procedure, ω_{GDD} is obtained from eq 5. Previous work indicates that the resulting value of ω_{GDD} is negligibly different from a fully self-consistent determination.[35]

Our valence excitation data set consists of 21 transitions assembled by Peach et al.[47] (Table S2), which has elsewhere been used to test LRC functionals.[15,46] Geometries and other properties for this data set can be found in ref 61. The CT data set (Table S1) is assembled from ref 47 and a newer data set of intramolecular CT transitions in ref 48. TD-DFT calculations for these two data sets employ full linear response, i.e., the TDA is not invoked. This helps to identify the transitions in question as compared to published benchmarks. These calculations use the def2-TZVPD basis set[74] and all DFT calculations use the SG-1 quadrature grid.[75] We do employ the TDA for the calculations on conjugated polymers, for the open-shell test set, and for the e^-(aq) models. Acene calculations use the def2-TZVPD basis set but for the conjugated polymers we use def2-ma-SVP.[76] The latter basis affords essentially identical ω_{IE} values for the acenes; see Tables S4 and S5.

■ ASSOCIATED CONTENT

Supporting Information

The Supporting Information is available free of charge at https://pubs.acs.org/doi/10.1021/acs.jpclett.5c00086.

Additional calculations and data (PDF)

Coordinates for the systems examined (ZIP)

■ AUTHOR INFORMATION

Corresponding Author

John M. Herbert − *Department of Chemistry & Biochemistry, The Ohio State University, Columbus, Ohio 43210, United States;* orcid.org/0000-0002-1663-2278; Email: herbert@chemistry.ohio-state.edu

Author

Aniket Mandal − *Department of Chemistry & Biochemistry, The Ohio State University, Columbus, Ohio 43210, United States;* orcid.org/0009-0000-8880-0122

Complete contact information is available at: https://pubs.acs.org/10.1021/acs.jpclett.5c00086

Notes

The authors declare the following competing financial interest(s): J.M.H. is part owner of Q-Chem Inc. and serves on its board of directors.

■ ACKNOWLEDGMENTS

This work was supported by National Science Foundation grant nos. CHE-1955282 and CHE-2402361. Calculations were performed at the Ohio Supercomputer Center.[77]

■ REFERENCES

(1) Herbert, J. M. Density-functional theory for electronic excited states. In *Theoretical and Computational Photochemistry: Fundamentals, Methods, Applications and Synergy with Experimental Approaches*; García-Iriepa, C., Marazzi, M., Eds.; Elsevier: 2023; Chapter 3, pages 69−118.

(2) Tozer, D. J.; Amos, R. D.; Handy, N. C.; Roos, B. O.; Serrano-Andrés, L. Does density functional theory contribute to the understanding of excited states of unsaturated organic compounds? *Mol. Phys.* **1999**, *97*, 859−868.

(3) Casida, M. E.; Gutierrez, F.; Guan, J.; Gadea, F.-X.; Salahub, D.; Daudey, J.-P. Charge-transfer correction for improved time-dependent local density approximation excited-state potential energy curves: Analysis within the two-level model with illustration for H_2 and LiH. *J. Chem. Phys.* **2000**, *113*, 7062−7071.

(4) Dreuw, A.; Weisman, J. L.; Head-Gordon, M. Long-range charge-transfer excited states in time-dependent density functional theory require non-local exchange. *J. Chem. Phys.* **2003**, *119*, 2943−2946.

(5) Dreuw, A.; Head-Gordon, M. Failure of time-dependent density functional theory for long-range charge-transfer excited-states: The zincbacteriochlorin−bacteriochlorin and bacteriochlorophyll−spheroidene complexes. *J. Am. Chem. Soc.* **2004**, *126*, 4007−4016.

(6) Magyar, R. J.; Tretiak, S. Dependence of spurious charge-transfer excited states on orbital exchange in TDDFT: Large molecules and clusters. *J. Chem. Theory Comput.* **2007**, *3*, 976−987.

(7) Lange, A.; Herbert, J. M. Simple methods to reduce charge-transfer contamination in time-dependent density-functional calculations of clusters and liquids. *J. Chem. Theory Comput.* **2007**, *3*, 1680−1690.

(8) Lange, A. W.; Rohrdanz, M. A.; Herbert, J. M. Charge-transfer excited states in a π-stacked adenine dimer, as predicted using long-range-corrected time-dependent density functional theory. *J. Phys. Chem. B* **2008**, *112*, 6304−6308.

(9) Tozer, D. J.; Handy, N. C. Improving virtual Kohn−Sham orbitals and eigenvalues: Application to excitation energies and static polarizabilities. *J. Chem. Phys.* **1998**, *109*, 10180−10189.

(10) Tozer, D. J.; Handy, N. C. On the determination of excitation energies using density functional theory. *Phys. Chem. Chem. Phys.* **2000**, *2*, 2117−2121.

(11) Tozer, D. J.; Handy, N. C. The importance of the asymptotic exchange-correlation potential in density functional theory. *Mol. Phys.* **2003**, *101*, 2669−2675.

(12) Iikura, H.; Tsuneda, T.; Yanai, T.; Hirao, K. A long-range correction scheme for generalized-gradient-approximation exchange functionals. *J. Chem. Phys.* **2001**, *115*, 3540−3544.

(13) Tawada, Y.; Tsuneda, T.; Yanagisawa, S.; Yanai, T.; Hirao, K. A long-range corrected time-dependent density functional theory. *J. Chem. Phys.* **2004**, *120*, 8425−8433.

(14) Tsuneda, T.; Hirao, K. Long-range correction for density functional theory. *Wiley Interdiscip. Rev.: Comput. Mol. Sci.* **2014**, *4*, 375−390.

(15) Rohrdanz, M. A.; Herbert, J. M. Simultaneous benchmarking of ground- and excited-state properties with long-range-corrected density functional theory. *J. Chem. Phys.* **2008**, *129*, 034107.

(16) Baer, R.; Neuhauser, D. Density functional theory with correct long-range asymptotic behavior. *Phys. Rev. Lett.* **2005**, *94*, 043002.

(17) Stein, T.; Kronik, L.; Baer, R. Reliable prediction of charge transfer excitations in molecular complexes using time-dependent density functional theory. *J. Am. Chem. Soc.* **2009**, *131*, 2818−2820.

(18) Stein, T.; Kronik, L.; Baer, R. Prediction of charge-transfer excitations in coumarin-based dyes using a range-separated functional tuned from first principles. *J. Chem. Phys.* **2009**, *131*, 244119.

(19) Baer, R.; Livshits, E.; Salzner, U. Tuned range-separated hybrids in density functional theory. *Annu. Rev. Phys. Chem.* **2010**, *61*, 85−109.

(20) Kronik, L.; Stein, T.; Refaely-Abramson, S.; Baer, R. Excitation gaps of finite-sized systems from optimally-tuned range-separated hybrid functionals. *J. Chem. Theory Comput.* **2012**, *8*, 1515−1531.

(21) Autschbach, J.; Srebro, M. Delocalization error and "functional tuning" in Kohn-Sham calculations of molecular properties. *Acc. Chem. Res.* **2014**, *47*, 2592−2602.

(22) Körzdörfer, T.; Brédas, J.-L. Organic electronic materials: Recent advances in the DFT description of the ground and excited states using tuned range-separated hybrid functionals. *Acc. Chem. Res.* **2014**, *47*, 3284−3291.

(23) Perdew, J. P.; Parr, R. G.; Levy, M.; Balduz, J. L., Jr. Density-functional theory for fractional particle number: Derivative discontinuities of the energy. *Phys. Rev. Lett.* **1982**, *49*, 1691−1694.

(24) Perdew, J. P.; Levy, M. Comment on "Significance of the highest occupied Kohn-Sham eigenvalue. *Phys. Rev. B* **1997**, *56*, 16021−16028.

(25) Kümmel, S. Charge-transfer excitations: A challenge for time-dependent density functional theory that has been met. *Adv. Energy Mater.* **2017**, *7*, 1700440.

(26) Hapka, M.; Rajchel, L.; Modrzejewski, M.; Chałasiȟski, G.; Szczęśniak, M. M. Tuned range-separated hybrid functionals in the symmetry-adapted perturbation theory. *J. Chem. Phys.* **2014**, *141*, 134120.

(27) Rudberg, E.; Rubensson, E. H.; Sałek, P. Kohn−Sham density functional theory electronic structure calculations with linearly scaling computational time and memory usage. *J. Chem. Theory Comput.* **2011**, *7*, 340−350.

(28) Rudberg, E. Difficulties in applying pure Kohn−Sham density functional theory electronic structure methods to protein molecules. *J. Phys.: Condens. Matt.* **2012**, *24*, 072202.

(29) Antony, J.; Grimme, S. Fully *ab initio* protein-ligand interaction energies with dispersion corrected density functional theory. *J. Comput. Chem.* **2012**, *33*, 1730−1739.

(30) Kulik, H. J.; Luehr, N.; Ufimtsev, I. S.; Martinez, T. J. Ab initio quantum chemistry for protein structures. *J. Phys. Chem. B* **2012**, *116*, 12501−12509.

(31) Grimme, S.; Hujo, W.; Kirchner, B. Performance of dispersion-corrected density functional theory for the interactions in ionic liquids. *Phys. Chem. Chem. Phys.* **2012**, *14*, 4875−4883.

(32) Isborn, C. M.; Mar, B. D.; Curchod, B. F. E.; Tavernelli, I.; Martínez, T. J. The charge transfer problem in density functional theory calculations of aqueously solvated molecules. *J. Phys. Chem. B* **2013**, *117*, 12189−12201.

(33) Lever, G.; Cole, J. D.; Hine, N. D. M.; Haynes, P. D.; Payne, M. C. Electrostatic considerations affecting the calculated HOMO-LUMO gap in protein molecules. *J. Phys.: Condens. Matt.* **2013**, *25*, 152101.

(34) Cole, D. J.; Hine, N. D. M. Applications of large-scale density functional theory in biology. *J. Phys.: Condens. Matt.* **2016**, *28*, 393001.

(35) Modrzejewski, M.; Rajchel, Ł.; Chalasinski, G.; Szczesniak, M. M. Density-dependent onset of the long-range exchange: A key to donor−acceptor properties. *J. Phys. Chem. A* **2013**, *117*, 11580−11586.

(36) Körzdörfer, T.; Sears, J. S.; Sutton, C.; Brédas, J.-L. Long-range corrected hybrid functionals for π-conjugated systems: Dependence of the range-separation parameter on conjugation length. *J. Chem. Phys.* **2011**, *135*, 204107.

(37) de Queiroz, T. B.; Kümmel, S. Charge-transfer excitations in low-gap systems under the influence of solvation and conformational disorder: Exploring range-separation tuning. *J. Chem. Phys.* **2014**, *141*, 084303.

(38) Bois, J.; Körzdörfer, T. Size-dependence of nonempirically tuned DFT starting points for G_0W_0 applied to π-conjugated molecular chains. *J. Chem. Theory Comput.* **2017**, *13*, 4962−4971.

(39) Gray, M.; Herbert, J. M. Simplified tuning of long-range corrected density functionals for symmetry-adapted perturbation theory. *J. Chem. Phys.* **2021**, *155*, 034103.

(40) Yang, B.; Yi, Y.; Zhang, C.-R.; Aziz, S. G.; Coropceanu, V.; Brédas, J.-L. Impact of electron delocalization on the nature of the charge-transfer states in model pentacene/C_{60} interfaces: A density functional theory study. *J. Phys. Chem. C* **2014**, *118*, 27648−27656.

(41) Uhlig, F.; Herbert, J. M.; Coons, M. P.; Jungwirth, P. Optical spectroscopy of the bulk and interfacial hydrated electron from ab initio calculations. *J. Phys. Chem. A* **2014**, *118*, 7507−7515.

(42) Wing, D.; Ohad, G.; Haber, J. B.; Filip, M. R.; Gant, S. E.; Neaton, J. B.; Kronik, L. Band gaps of crystalline solids from Wannier-localization−based optimal tuning of a screened range-separated hybrid functional. *Proc. Natl. Acad. Sci. U.S.A.* **2021**, *118*, No. e2104556118.

(43) Ohad, G.; Hartstein, M.; Gould, T.; Neaton, J. B.; Kronik, L. Nonempirical prediction of the length-dependent ionization potential in molecular chains. *J. Chem. Theory Comput.* **2024**, *20*, 7168−7175.

(44) Lao, K. U.; Herbert, J. M. Atomic orbital implementation of extended symmetry-adapted perturbation theory (XSAPT) and benchmark calculations for large supramolecular complexes. *J. Chem. Theory Comput.* **2018**, *14*, 2955−2978.

(45) Carter-Fenk, K.; Mundy, C. J.; Herbert, J. M. Natural charge-transfer analysis: Eliminating spurious charge-transfer states in time-dependent density functional theory via diabatization, with application to projection-based embedding. *J. Chem. Theory Comput.* **2021**, *17*, 4195−4210.

(46) Rohrdanz, M. A.; Martins, K. M.; Herbert, J. M. A long-range-corrected density functional that performs well for both ground-state properties and time-dependent density functional theory excitation energies, including charge-transfer excited states. *J. Chem. Phys.* **2009**, *130*, 054112.

(47) Peach, M. J. G.; Benfield, P.; Helgaker, T.; Tozer, D. J. Excitation energies in density functional theory: An evaluation and a diagnostic test. *J. Chem. Phys.* **2008**, *128*, 044118.

(48) Loos, P.-F.; Comin, M.; Blase, X.; Jacquemin, D. Reference energies for intramolecular charge-transfer excitations. *J. Chem. Theory Comput.* **2021**, *17*, 3666−3686.

(49) Lange, A. W.; Herbert, J. M. Both intra- and interstrand charge-transfer excited states in B-DNA are present at energies comparable to, or just above, the $^1\pi\pi^*$ excitonic bright states. *J. Am. Chem. Soc.* **2009**, *131*, 3913−3922.

(50) Richard, R. M.; Herbert, J. M. Time-dependent density-functional description of the ^1L_a state in polycyclic aromatic hydrocarbons: Charge-transfer character in disguise? *J. Chem. Theory Comput.* **2011**, *7*, 1296−1306.

(51) Alam, B.; Morrison, A. F.; Herbert, J. M. Charge separation and charge transfer in the low-lying excited states of pentacene. *J. Phys. Chem. C* **2020**, *124*, 24653−24666.

(52) Yanai, T.; Tew, D. P.; Handy, N. C. A new hybrid exchange-correlation functional using the Coulomb-attenuating method (CAM-B3LYP). *Chem. Phys. Lett.* **2004**, *393*, 51−57.

(53) Mester, D.; Kállay, M. Charge-transfer excitations within density functional theory: How accurate are the most recommended approaches? *J. Chem. Theory Comput.* **2022**, *18*, 1646−1662.

(54) Srebro, M.; Autschbach, J. Tuned range-separated time-dependent density functional theory applied to optical rotation. *J. Chem. Theory Comput.* **2012**, *8*, 245−256.

(55) Laurent, A. D.; Jacquemin, D. TD-DFT benchmarks: A review. *Int. J. Quantum Chem.* **2013**, *113*, 2019−2039.

(56) Grimme, S.; Parac, M. Substantial errors from time-dependent density functional theory for the calculation of excited states of large π systems. *ChemPhysChem* **2003**, *4*, 292−295.

(57) Carter-Fenk, K.; Herbert, J. M. Reinterpreting π-stacking. *Phys. Chem. Chem. Phys.* **2020**, *22*, 24870−24886.

(58) Bendikov, M.; Duong, H. M.; Starkey, K.; Houk, K. N.; Carter, E. A.; Wudl, F. Oligoacenes: Theoretical prediction of open-shell singlet diradical ground states. *J. Am. Chem. Soc.* **2004**, *126*, 7416−7417.

(59) Yang, Y.; Davidson, E. R.; Yang, W. Nature of ground and electronic excited states of higher acenes. *Proc. Natl. Acad. Sci. U.S.A.* **2016**, *113*, E5098−E5107.

(60) Plasser, F.; Thomitzni, B.; Bäppler, S. A.; Wenzel, J.; Rehn, D. R.; Wormit, M.; Dreuw, A. Statistical analysis of electronic excitation processes: Spatial location, compactness, charge transfer, and electron-hole correlation. *J. Comput. Chem.* **2015**, *36*, 1609−1620.

(61) Herbert, J. M.; Mandal, A. Importance or orbital invariance in quantifying electron−hole separation and exciton size. *J. Chem. Theory Comput.* **2024**, *20*, 9446−9463.

(62) Mewes, S. A.; Plasser, F.; Dreuw, A. Universal exciton size in organic polymers is determined by nonlocal orbital exchange in time-dependent density functional theory. *J. Phys. Chem. Lett.* **2017**, *8*, 1205−1210.

(63) Yan, T.; Bonardi, A.; Adamo, C.; Ciofini, I. Adaptable range-separated hybrids for the description of excited states: Tuning the range separation parameter on effective charge transfer distance. *J. Chem. Theory Comput.* **2025**, *21*, 1892.

(64) Loos, P.-F.; Scemama, A.; Boggio-Pasqua, M.; Jacquemin, D. Mountaineering strategy to excited states: Highly accurate energies and benchmarks for exotic molecules and radicals. *J. Chem. Theory Comput.* **2020**, *16*, 3720−3736.

(65) Herbert, J. M. Structure of the aqueous electron. *Phys. Chem. Chem. Phys.* **2019**, *21*, 20538−20565.

(66) Jacobson, L. D.; Herbert, J. M. Polarization-bound quasi-continuum states are responsible for the 'blue tail' in the optical absorption spectrum of the aqueous electron. *J. Am. Chem. Soc.* **2010**, *132*, 10000−10002.

(67) Herbert, J. M.; Jacobson, L. D. Structure of the aqueous electron: Assessment of one-electron pseudopotential models in comparison to experimental data and time-dependent density functional theory. *J. Phys. Chem. A* **2011**, *115*, 14470−14483.

(68) Carter-Fenk, K.; Johnson, B. A.; Herbert, J. M.; Schenter, G. K.; Mundy, C. J. Birth of the hydrated electron via charge-transfer-to-solvent excitation of aqueous iodide. *J. Phys. Chem. Lett.* **2023**, *14*, 870−878.

(69) Herbert, J. M.; Coons, M. P. The hydrated electron. *Annu. Rev. Phys. Chem.* **2017**, *68*, 447−472.

(70) Carter-Fenk, K.; Lao, K. U.; Herbert, J. M. Predicting and understanding non-covalent interactions using novel forms of symmetry-adapted perturbation theory. *Acc. Chem. Res.* **2021**, *54*, 3679−3690.

(71) Epifanovsky, E.; et al. Software for the frontiers of quantum chemistry: An overview of developments in the Q-Chem 5 package. *J. Chem. Phys.* **2021**, *155*, 084801.

(72) Becke, A. D.; Edgecombe, K. E. A simple measure of electron localization in atomic and molecular systems. *J. Chem. Phys.* **1990**, *92*, 5397−5403.

(73) Schmider, H. L.; Becke, A. D. Chemical content of the kinetic energy density. *J. Mol. Struct. (Theochem)* **2000**, *527*, 51−61.

(74) Rappoport, D.; Furche, F. Property-optimized Gaussian basis sets for molecular response calculations. *J. Chem. Phys.* **2010**, *133*, 134105.

(75) Gill, P. M. W.; Johnson, B. G.; Pople, J. A. A standard grid for density-functional calculations. *Chem. Phys. Lett.* **1993**, *209*, 506−512.

(76) Gray, M.; Herbert, J. M. Comprehensive basis-set testing of extended symmetry-adapted perturbation theory and assessment of mixed-basis combinations to reduce cost. *J. Chem. Theory Comput.* **2022**, *18*, 2308−2330.

(77) Ohio Supercomputer Center, https://osc.edu/ark:/19495/f5s1ph73 (accessed 2024-02-23).